Development of Ruthenium Antitumor Drugs that Overcome Multidrug Resistance Mechanisms

Carsten A. Vock,[†] Wee Han Ang,[†] Claudine Scolaro,[†] Andrew D. Phillips,[†] Lucienne Lagopoulos,[‡] Lucienne Juillerat-Jeanneret,*[,‡] Gianni Sava,[§,||] Rosario Scopelliti,[†] and Paul J. Dyson*[,†]

Institut des Sciences et Ingénierie Chimiques, Ecole Polytechnique Fédérale de Lausanne (EPFL), CH-1015 Lausanne, Switzerland, University Institute of Pathology, Centre Hospitalier Universitaire Vaudois (CHUV), CH-1011 Lausanne, Switzerland, Callerio Foundation Onlus, Via A. Fleming 22-31, 34127, Trieste, Italy, and Dipartimento di Scienze Biomediche, Università di Trieste, Via L. Giorgieri 7-9, 34127, Trieste, Italy

Received January 11, 2007

Organometallic ruthenium(II) complexes of the general formula [Ru(η^6-*p*-cymene)Cl_2(L)] and [Ru(η^6-*p*-cymene)Cl$(L)_2$][BPh_4] with modified phenoxazine- and anthracene-based multidrug resistance (MDR) modulator ligands (L) have been synthesized, spectroscopically characterized, and evaluated in vitro for their cytotoxic and MDR reverting properties in comparison with the free ligands. For an anthracene-based ligand, coordination to a ruthenium(II) arene fragment led to significant improvement of cytotoxicity as well as Pgp inhibition activity. A similar, but weaker effect was also observed when using a benzimidazole-phenoxazine derivative as Pgp inhibitor. The most active compound in terms of both Pgp inhibition and cytotoxicity is [Ru(η^6-*p*-cymene)Cl_2(L)], where L is an anthracene-based ligand. Studies show that it induces cell death via inhibition of DNA synthesis. Moreover, because the complex is fluorescent, its uptake in cells was studied, and relative to the free anthracene-based ligand, uptake of the complex is accelerated and accumulation of the complex in the cell nucleus is observed.

Introduction

Drug resistance, that is, the appearance of reduced or missing response of microorganisms as well as cancer cells to applied chemotherapeutic agents, is a serious problem for the treatment of different diseases.[1] The macroscopic phenomenon can be divided into intrinsic drug resistance, where the application of drugs has no effect at all, and acquired drug resistance, where a normal response is observed at the beginning of the therapy, which then diminishes quickly and often disappears completely after a certain period of time.[2,3] For the treatment of cancer, but other diseases also, multidrug resistance (MDR[a]) plays a very important role. MDR corresponds to a particular form of drug resistance, characterized by the simultaneous appearance of resistance to the applied chemotherapeutic agent and cross-resistance to a number of functionally and structurally diverse hydrophobic drugs, with different mechanisms of action.[4,5]

The cellular mechanisms leading to MDR are still not fully understood,[6] and several factors seem to be of importance.[7] Most frequently discussed are (a) lowering of the intracellular concentration of the drug either by blocking uptake or increasing efflux,[8] (b) increased rates of repair of the drug damage,[9] and (c) accelerated rates of drug inactivation by protein binding (e.g., metallothionine and glutathione-S-transferase) and conjugation to small molecules such as glutathione.[10] It has been shown that MDR cells overexpress certain efflux proteins, which leads to a significantly lower intracellular level of chemotherapeutical agents.[11] The most prominent examples of this superfamily of proteins, for which a similar mechanism of action is assumed, are P-glycoprotein (Pgp) and MDR protein (MRP1).[12] While Pgp mainly transports neutral and charged molecules in unmodified form, MRP1 is also able to accept metabolized substrates such as GSH, glucuronide, or sulfate conjugates.[13−15] Because the transport into the extracellular medium has to be carried out against a strong concentration gradient, the process requires energy, and all the known MDR proteins are ATP-dependent efflux pumps.[16] Experimental results indicate that ATP- and substrate binding to Pgp occur independently.[17,18] However, ATP-binding and hydrolysis are necessary to mediate the transport.[19]

Due to the high importance of Pgp and MRPs for effective anticancer therapy, a lot of research has focused on developing MDR modulators, which function by blocking transporter-mediated drug efflux so that a concomitantly administered anticancer drug can cause tumor cell death. Interestingly, a huge structural variety is observed not only for the substrates, but also for the blockers of the MDR efflux proteins.

One of the most promising MDR antagonists is verapamil **1** (Figure 1), which was the first compound found to reverse MDR in vitro[20] and to reach clinical trials.[21] It has also been coadministered with ruthenium compounds, resulting in a significant improvement of their toxicity to cancer cells.[22] Interestingly, the (*R*)-enantiomer of verapamil **1** exhibits the same MDR reversal activity as the (*S*)-enantiomer, but shows lower cardiovascular side effects.[23,24] A number of pharmacologically active compounds, for example, the potassium channel blocker amiodarone,[25] the CNS active agent fluphenazine,[26] and the important immunosuppressant cyclosporin A[27] (for structures, see Supporting Information (SI)), have also been shown to be strong MDR reversal agents. However, due to their own strong pharmacological effects, these drugs are not suitable for coadministration with anticancer drugs.

* To whom correspondence should be addressed. Dr. Lucienne Juillerat-Jeanneret, University Institute of Pathology, CHUV, Rue de Bugnon 25, CH-1011 Lausanne, Switzerland. Tel.: +41 21 314 7173. Fax: +41 21 314 7115. E-mail: lucienne.juillerat@chuv.ch. Prof. Paul J. Dyson, Institut des Sciences et Ingénierie Chimiques, Ecole Polytechnique Fédérale de Lausanne (EPFL), CH-1015 Lausanne, Switzerland. Tel.: +41 (0)21 693 98 54. Fax: +41 (0)21 693 98 85. E-mail: paul.dyson@epfl.ch.

[†] Ecole Polytechnique Fédérale de Lausanne.

[‡] Centre Hospitalier Universitaire Vaudois.

[§] Callerio Foundation Onlus.

[||] Università di Trieste.

[a] Abbreviations: anthraimid, *N*-(anthracen-9-yl)-imidazole; EtOAc, ethyl acetate; MDR, multidrug resistance/resistant; MTT, 3-(4,5-dimethylthiazol-2-yl)-2,5-diphenyltetrazolium bromide; Pgp, P-glycoprotein; phenoximid, 2-(imidazol-1-yl)-1-(phenoxazin-10-yl)-ethanone; phenoxbenzimid, 2-(benzimidazol-1-yl)-1-(phenoxazin-10-yl)-ethanone; pta, 1,3,5-triaza-7-phosphaadamantane.

10.1021/jm070039f CCC: $37.00
Published on Web 04/10/2007

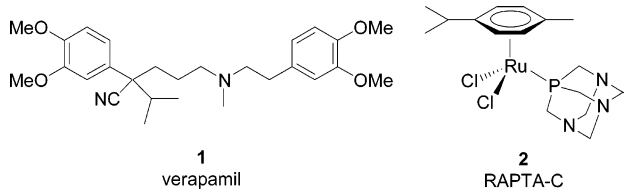

1 verapamil **2** RAPTA-C

Figure 1. Structures of verapamil **1** and RAPTA-C **2**.

A serious problem with the application of Pgp or MDR inhibitors in combination with cytotoxic anticancer agents is the non-specific expression of the efflux pumps in human bodies. Deleterious effects in vivo are possible because Pgp also occurs in normal tissues, such as adrenal, gravid uterus, kidney, liver, colon, and capillary endothelial cells in the brain.[28] On the other hand, ruthenium-based anticancer drugs exhibit a low general toxicity and specifically accumulate in cancer cells.[29] This is probably due, at least in part, to the ability of ruthenium to mimic iron in binding to certain biomolecules, including serum transferrin and albumin, which are known to be responsible for solubilization, transport, and detoxification of iron in mammals.[30] Rapidly growing cancer cells have a greater requirement for iron, which leads to an overexpression of transferrin receptors on their cell surfaces. In vivo experiments with radio-labeled ruthenium compounds have shown a 2−12-fold accumulation in cancer cells compared with that of healthy cells, depending on the cell type, indicating that the reduced toxicity of ruthenium anticancer compounds is due to their higher selectivity toward malignant cells.[31] During the last years, our group has studied the cytotoxic properties of a family of η^6-arene ruthenium(II) pta complexes (pta = 1,3,5-triaza-7-phosphaadamantane), with the parent compound being [Ru(η^6-*p*-cymene)Cl_2(pta)], termed RAPTA-C **2** (Figure 1).[32] The studies have shown a high selectivity of these compounds toward cancer cells. Accordingly, we decided to prepare compounds in which the benefits of the modulators are combined with the selectivity of ruthenium compounds toward cancer cells. Thus, we have synthesized ruthenium complexes with MDR modulators as ligands and evaluated the cytotoxic and MDR reversal properties of these new compounds in comparison with the free MDR modulators. The outcome of these studies are described herein.

Results and Discussion

Phenoxazine-based compounds, for example, **3** and **4** (Figure 2) developed by Thimmaiah et al.,[33] were chosen as MDR modulators for the investigations described herein. These derivatives have been shown to cause a 2.4-fold (for **3**) and 20.2-fold (for **4**) enrichment of vinblastine in MDR KBCh^R-8-5 cells.[33] It was not possible to attach **3** or **4** to a ruthenium center, and therefore, with respect to our recent research in the field of η^6-arene ruthenium(II) imidazole complexes,[34] we decided to modify the structures of the phenoxazine derivatives by introducing an imidazole or benzimidazole moiety to facilitate coordination (Figure 2). Following a procedure developed by Thimmaiah et al.,[33] **5** and **6** were synthesized by heating a mixture of **3** with an excess of KI and imidazole or benzimidazole in CH_3CN. Furthermore, derivative **7** was synthesized with the intention to substitute the potentially labile *N*-acylphenoxazine moiety by a stably bound anthracene group, while at the same time introducing potentially useful flurorescent properties. The synthesis of **7** was carried out via copper-catalyzed Ullmann-coupling in the presence of L-proline, following a procedure described by Ma and Cai.[35]

Compounds **5**−**7** were reacted with [Ru(η^6-*p*-cymene)Cl_2]$_2$ in CH_2Cl_2 at room temperature (rt) in a 2:1 ratio, leading to the monosubstituted complexes of type [Ru(η^6-*p*-cymene)Cl_2(L)] **8**, **9**, and **10** (Figure 2). Complexes **11** and **12** (Figure 2), as representative examples for the general class of monocharged bisimidazole ruthenium(II) complexes [Ru(η^6-*p*-cymene)Cl-$(L)_2]^+$, were obtained by treating a solution of [Ru(η^6-*p*-cymene)Cl_2]$_2$ and the calculated amount of **5** or **7** in MeOH with a slight excess of $NaBPh_4$ at rt or under reflux. However, their poor solubility in aqueous media even in the presence of DMSO precluded their biological evaluation. Several attempts to synthesize the corresponding bisbenzimidazole derivative using **6** failed, presumably due to increased steric hindrance, supported by the crystal structures, which show the possibility of sterically less demanding conformations when imidazole derivatives are used (see Crystallographic Analysis of **9**, **10**, and **12** and SI).

The ^{1}H NMR spectra of ligands **5**−**7** and complexes **8**−**12** (NMR numbering scheme, see SI) show some notable features. The resonances for the protons N-C*H*-N in ligands **5**−**7** are shifted strongly by $\Delta\delta \sim 0.5$ ppm to higher frequencies in complexes **8**−**10**. The same, but weaker tendency is also observed for the 4′-H resonances in **5** and **7**. For **12**, a double set of peaks is observed for the anthracene systems in the ^{1}H and ^{13}C NMR spectra, indicating an interaction of the bulky aromatic substituents with each other as well as a reduced ability to rotate. This observation is supported by crystallographic data (see below). For the anthracene-based systems **7**, **10**, and **12**, the ^{13}C NMR resonance of the quaternary carbon attached to the nitrogen in the imidazole system is very weak and could only be detected for compound **12** after a prolonged experiment time.

The ESI mass spectra of the ligands **5**−**7** in methanol/0.1% formic acid provide parent peaks corresponding to the protonated cations for all compounds. For the monoligated complexes **8**−**10** in CH_3CN, the most intensive peak always corresponds to a monocationic species obtained by the loss of one chloride ligand. For **11** and **12**, the most intensive peak corresponds to the parent ion [Ru(cymene)Cl$(L)_2]^+$.

Crystallographic Analysis of 9, 10, and 12. Single crystals suitable for X-ray diffraction were obtained for **8**, **9**, **10**, and **12**. However, in the case of **8**, a poor quality dataset (final weighted *R* factor (R_w) is 19%) was collected due to the extremely small size of the crystal (see Figure S5, SI). The solution confirms the atomic type, general connectivity, and orientation of the substituents within the molecule, but metric parameters are not comparable with the other structures. Complex **9** contains a nondisordered ethyl acetate solvate within the unit cell (Figure 3), which has a relatively short interaction of 2.35 Å, with the central hydrogen of the benzimidazole ligand. All the structures feature the typical three-legged piano-type structure about the metal center. Both **9** and **10**, which contain a single N-substituted imidazole ligand, represent the only crystallographically characterized arene-ruthenium species of this type. The metric parameters of the acetylphenoxazine component in **9** match almost exactly those of other structures such as **4**, including the typical folding pattern of the ligand along the N3−O2 vector (Figure 4). One of the most striking aspects of the crystal packing occurs for species **12**, where parallel π-stacking interactions are observed between the opposite anthracene groups of the imidazole ligands (Figure S4, SI). The ligands are stacked by rotation about the center of anthracence, with a separation distance of about 3.36 Å (Figure 5).

Results of the Biological Evaluation. The MDR inhibitors **5**−**7** and the corresponding complexes **8**−**10** were evaluated

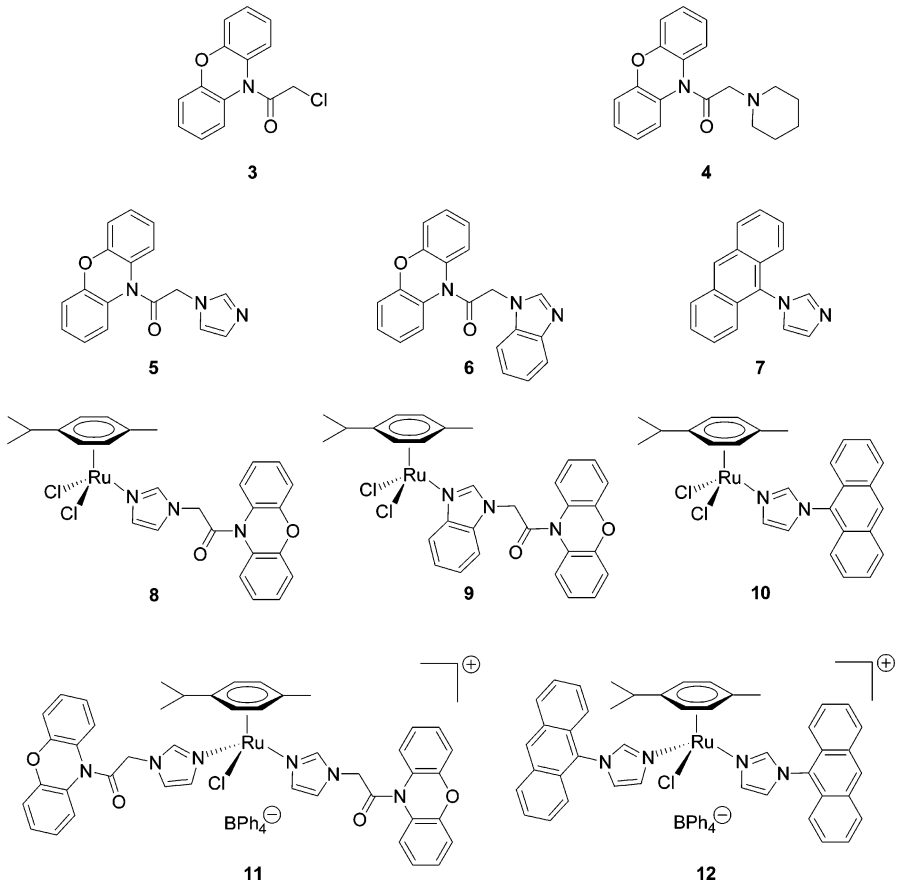

Figure 2. Structures of the known MDR modulators **3** and **4**, the new derivatives/analogues **5**−**7**, and the complexes **8**−**12**.

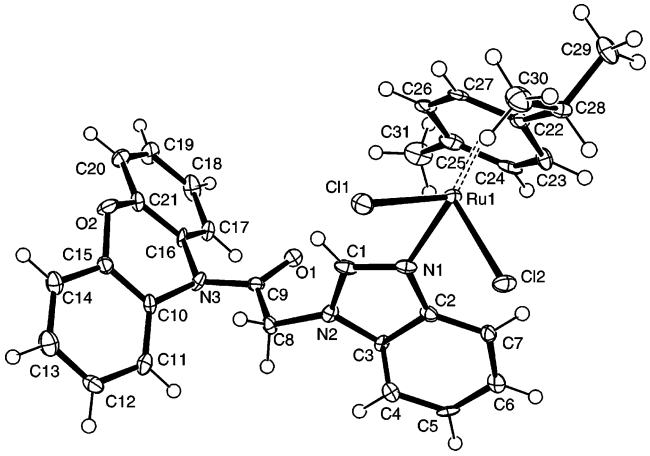

Figure 3. ORTEP plot of **9** (ethyl acetate solvent omitted for clarity) drawn with 50% probability ellipsoids. Selected bond lengths (Å), angles and torsion angles (°): Ru−Cl1, 2.424(2); Ru−Cl2, 2.445(2); Ru1−N1, 2.122(5); Ru−Ar(centriod), 1.662; N2−C8, 1.461(8); O1−C9, 1.225(8); N3−C9, 1.400(9); Cl1−Ru1−Cl2, 87.25(7); N1−Ru1−Cl1, 85.54(16); N1−Ru1−Cl2, 86.75(16); Ar(centriod)−Ru1−N1, 128.05; Ar(centriod)−Ru1−Cl1, 126.99; Ar(centriod)−Ru1−Cl2, 128.02; O1−C9−N3, 121.9(7); Ru−Ar(centriod)−N1−C1, −93.82; N2−C8−C9−O1, 15.8(9); N2−C8−C9−N3, −165.8(6); C16−N3−C9−O1, −168.9(6).

in a comparative in vitro MTT cell viability assay[36] with four tumorigenic and one nontumorigenic cell lines. The results can be interpreted as an indicator for the cytotoxic selectivity of the applied drug toward tumorigenic tissues.[32b,d] The IC_{50} values for compounds **3** and **5**−**10** are depicted in Table 1. For the ligands **5**−**7**, the data indicate **5** to be the most cytotoxic derivative in three of the five tested cell lines, although the cytotoxicity is much lower in A549 and T47D cells. Compounds **6** and **7** show a more consistent profile across the panel of cell lines, both of them having a comparatively very low effect in the nontumorigenic HBL-100 cells. The general toxicity of complexes **8**−**10** is in the same order of magnitude as for the ligands **5**−**7**, with **10** being the most and **8** being the least cytotoxic substance. In addition, **10** provides a relatively homogeneous cytotoxicity profile across the panel of cell lines, showing similar activity in all tumorigenic cell lines and the nontumorigenic cell line HBL-100, which could be an indicator for a generalized mechanism of action. Interestingly, **8** exhibits highly cytotoxic properties only in HT29 cells and is, therefore, at least in terms of selectivity toward certain types of cancer, also a promising compound.

The A549 lung carcinoma, HT29 colon carcinoma, and T47D breast carcinoma cell lines were screened for Pgp activity, using Calcein-AM as the substrate, following a protocol described by Weiss et al.[37] Both A549 and HT29 exhibited significantly higher Pgp activity compared to T47D; thus, A549 was used as the cell line to evaluate the Pgp-inhibitory activity of the drugs (Figure 6). Two parameters of Pgp inhibition, the concentration required to double the baseline fluorescence level ($F_{2.0}$) and the relative inhibition of the compounds at a concentration of 80 μM compared to verapamil **1**, are shown in Table 2. An incubation time of 60 min was used so that the results were not compromised by cell death.

It is observed that the benzimidazole derivative **6** is the best Pgp inhibitor in the series of ligands **5**−**7**, although it is somewhat less active than **1**, which was used as reference. The imidazole derivative **5** and the anthracene compound **7** exhibit significantly weaker Pgp inhibition activity. For the complexes **8**−**10**, a loss of Pgp activity can be observed for **8** and **9** in comparison with that of the corresponding free ligands **5** and

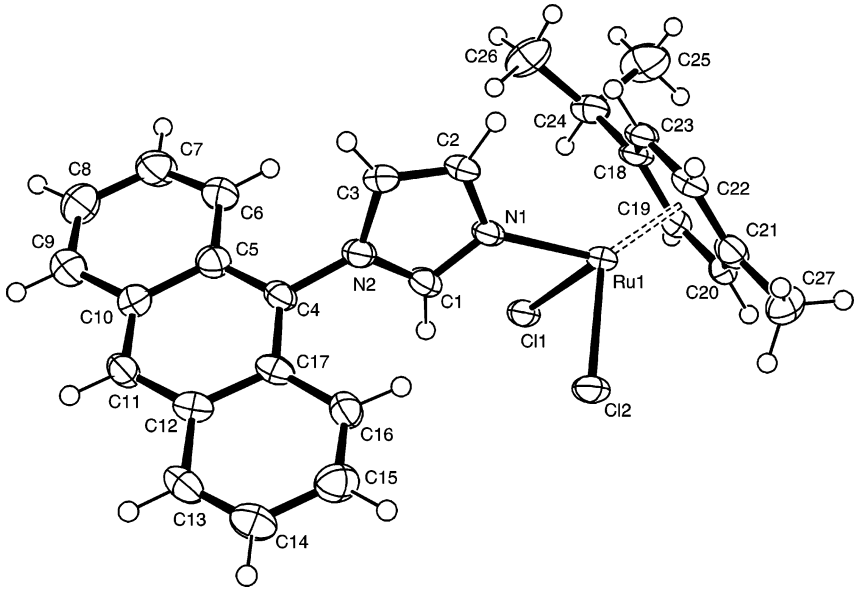

Figure 4. ORTEP plot of **10** drawn with 50% probability ellipsoids. Selected bond lengths (Å), angles, and torsion angles (°): Ru1−Cl1, 2.4275-(16); Ru1−Cl2, 2.4394(15); Ru1−N1, 2.142(5); N2−C4, 1.455(7); Ru1−Ar(centriod), 1.672; Cl1−Ru1−Cl2, 88.24(5); N1−Ru1−Cl1, 85.14(14); N1−Ru1−Cl2, 83.93(13); C1−N1−Ru1, 122.9(4); Ar(centroid)−Ru1−N1, 131.92; Ar(centriod)−Ru1−Cl1, 128.43; Ar(centriod)−Ru1−Cl2, 124.29; Ar(centriod)−Ru1−N1−C1, 169.02; C1−N2−C4−C5, −113.3(7); C1−N2−C4−C17, 67.9(8).

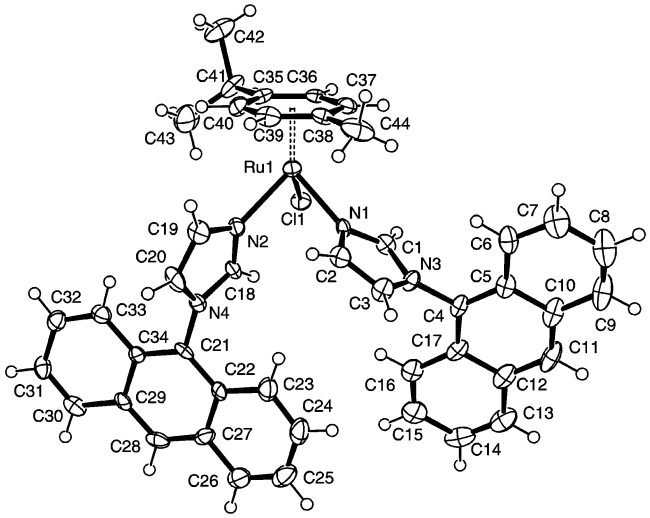

Figure 5. ORTEP plot of **12** (BPh_4 counterion omitted for clarity) drawn with 50% probability ellipsoids. Selected bond lengths (Å), angles, and torsion angles (°): Ru1−Cl1, 2.3863(9); Ru1−N1, 2.115-(3); Ru1−N2, 2.119(3); Ru1−Ar(centriod), 1.663; N3−C4, 1.451(4); N4−C21, 1.443(4); N1−Ru1−Cl1, 87.27(7); N2−Ru1−Cl1, 87.36-(8); N1−Ru1−N2, 82.23(10); Ar(centriod)−Ru1−Cl1, 125.31; Ar-(centriod)−Ru1−N1, 128.75; Ar(centriod)−Ru1−N2, 130.92; Ar-(centriod)−Ru1−N1−C1, −92.37; Ar(centriod)−Ru1−N1−C1, −92.37; Ar(centriod)−Ru1−N2−C18, 159.61; C1−N3−C4−C5, 95.3(4); C18−N4−C21−C34, −111.2(4).

6. Interestingly, the Pgp inhibition activity of complex **10** is strongly increased in comparison with that of the free ligand **7**, now approaching the levels of verapamil **1**. The Pgp inhibition activity for **8**−**10** correlates well with the activity of the compounds to inhibit cell growth and with the lipophilicity of the compounds, with **8** being the least and **10** being the most lipophilic derivatives. For **5**−**7**, however, there is no clear correlation between cytotoxicity and Pgp inhibition activity; the most lipophilic derivative **7** turns out to be the weakest inhibitor of cell growth proliferation, while the most hydrophilic ligand **5** is the most toxic derivative.

To determine the mode of cytotoxicity for the most promising complex **10**, A549 cells were exposed to the drug for 6 and 8 h; the cell viability was measured using the Alamar Blue assay, which determines the mitochondrial activity of the exposed cells, and ^{3}H-thymidine incorporation assay, which determines the level of DNA synthesis within the cells (Figure 7). From these experiments, it appears that inhibition of DNA synthesis on exposure to **10** precedes cell death, suggesting that the inhibition of DNA synthesis to be a probable trigger for apoptosis/necrosis.

Due to the fluorescence properties of the anthracene-based ligand **7**, and to a weaker extent of the complex **10** (Figure 8), the effect of these compounds on A549 lung carcinoma cells were studied by fluorecence microscopy (Figure 9). Drug accumulation was detected in the cells exposed to complex **10** as early as 30 min after drug application, whereas significant drug accumulation was only detected in cells exposed to ligand **7** after 1 h of exposure. This difference in uptake could explain the earlier observation that ligand **7** is a poor Pgp-inhibitor compared to **10**, because the calcein fluorescence levels were measured within 60 min of drug exposure. It was also observed that at each time interval, the fluorescence levels of cells exposed to **7** is significantly lower than that of **10**, suggesting that **10** was taken up more readily. In addition, it was observed that **10** accumulated in the cell nucleus after 1 h of exposure, whereas **7** accumulated in the cytosol and organelles. The accumulation of ruthenium in the nucleus has already been described for the phase II clinical trial drug KP1019.[30b] The accumulation of **10** in the cell nucleus is also consistent with the observation that inhibition of DNA synthesis was responsible for subsequent cell death in A549 cells exposed to complex **10**.

Conclusions

Three new phenoxazine- and anthracene-based Pgp inhibitors **5**−**7** containing an imidazole moiety and their water-soluble ruthenium(II) arene derivatives **8**−**12** were prepared and characterized. The ligands **5**−**7** and their monoligated complexes **8**−**10** were evaluated for their cytotoxic and Pgp inhibiting properties. Remarkably, in the case of **7**, coordination to the ruthenium(II) center leads to a strong increase in cytotoxicity, similarly, although to a lesser extent, this behavior is observed for **6**. Pgp inhibition studies revealed **10** to be the most powerful Pgp inhibitor. In comparison, ligand **7** showed only minor Pgp

Table 1. IC_{50} Values of Ligands **5**−**7**, Complexes **8**−**10**, and Reference Compounds **2** and **3** on Tumorigenic and Nontumorigenic Cell Lines after 72 h of Incubation, Determined Using the MTT Assay

	tumorigenic cell lines IC_{50} [μM]				nontumorigenic cell lines
compounds	A549	HT29	T47D	TS/A	HBL-100
RAPTA-C **2**	>100	>100	>100	>100	>100
3	>100	11	7	40	29
phenoximid (**5**)	>100	17	95	30	23
phenoxbenzimid (**6**)	75	33	91	51	>100
anthraimid (**7**)	75	45	34	101	221
[Ru(η^6-*p*-cymene)Cl_2(phenoximid)] (**8**)	>100	22	94	75	>100
[Ru(η^6-*p*-cymene)Cl_2(phenoxbenzimid)] (**9**)	80	43	71	40	91
[Ru(η^6-*p*-cymene)Cl_2(anthraimid)] (**10**)	37	37	22	23	21

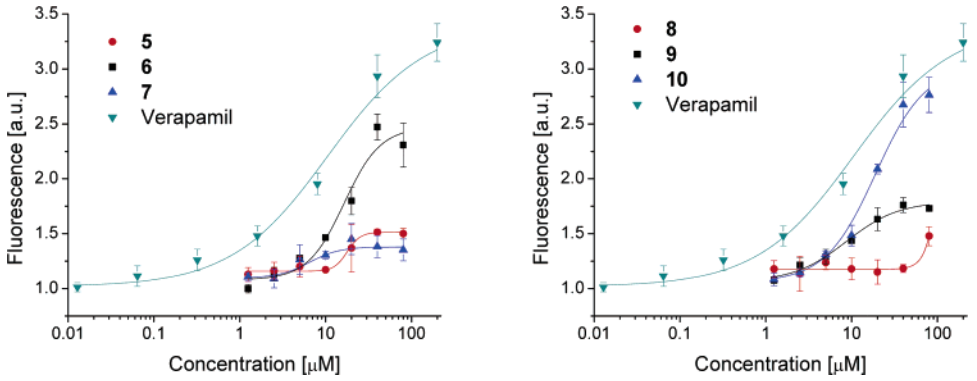

Figure 6. Results of the calcein-AM uptake assays in A549 cells for **5**−**7** (left) and **8**−**10** (right); verapamil was used as the reference.

Table 2. Pgp Inhibition Parameters of the Complexes on A549 Lung Carcinoma after 60 min of Incubation

compounds	$F_{2.0}$[a] (μM)	% inhibition[b] (at 80 μM)
verapamil (**1**)	7	100
phenoximid (**5**)	>100	24
phenoxbenzimid (**6**)	23	65
anthraimid (**7**)	>100	18
[Ru(η^6-*p*-cymene)Cl_2(phenoximid)] (**8**)	>100	25
[Ru(η^6-*p*-cymene)Cl_2(phenoxbenzimid)] (**9**)	>100	37
[Ru(η^6-*p*-cymene)Cl_2(anthraimid)] (**10**)	18	88

[a] Concentration at which the fluorescence values are doubled (compared to baseline). [b] Relative inhibition (compared to verapamil) at 80 μM drug concentration.

inhibition potential. Fluorescence microscopy studies in cells indicate that this might be due to reduced uptake. For both other pairs of compounds **5**/**8** and **6**/**9**, the ability to inhibit Pgp efflux proteins decreases from free ligand to complex, although for complex **8**, the cytotoxicity data show an increase in selectivity toward HT29 cells in comparison with the ligand **5**. For the most promising complex **10**, it was found that inhibition of DNA synthesis is a possible mechanism of cytotoxic action, supported by the results of ^{3}H-thymidine incorporation assay and fluorescence spectroscopy. These observations correlate well with the general toxicity of **10** across the panel of cell lines, which indicates that, although the Pgp inhibition potential of **10** has been confirmed, the main mechanism of action might be independent from inhibition of efflux proteins. Possibly the polyaromatic system of the anthracene ligand **7** might act as a DNA intercalator, and its coordination to a ruthenium center facilitates cellular uptake.

It has previously been shown that combining derivatives of known drugs to organometallic fragments can have a dramatic effect on their activity.[38] Notably, Jaouen and co-workers have shown that the efficacy of tamoxifen (an organic drug that blocks the estrogen hormone receptor site in hormone-dependent breast cancers) can be modified/improved by incorporation of the ferrocenyl group or other metal-based units.[39] A related strategy, that is, attachment of a ferrocenyl group to the antimalaria drug chloroquine, has proven highly successful, such that the modified derivative is able to overcome parasite resistance to the organic drug.[40] The problem of drug targeting and/or resistance has also been addressed with platinum-based anticancer drugs. Specifically, Lippard has demonstrated that a Pt(IV)−estrogen complex, formed by conjugating an estrogen derivative via a succinate linker onto a *trans*-Pt(IV) carboxylate structure, was able to sensitize estrogen-receptor(+) mammalian tumor cells to treatment.[41] We have also shown that a Pt(IV)−ethacrynic acid complex could inhibit the activity of glutathione-S-transferase, an enzyme related to resistance in certain cancer types in vitro.[42] Meggers has also used attached kinase GSK-3 inhibitors to ruthenium fragments and has developed some related strategies combining active organic molecules with ruthenium centers that show considerable promise.[43] Here, however, we demonstrate that synergistic effects are observed when combining Pgp inhibitors with organoruthenium fragments, and, in the case of **10**, coordination of the organic ligand to the ruthenium(II)-arene unit induces Pgp inhibition. Although it is still too early to generalize this observation, we have shown for the first time the considerable potential of combinational metal-based anticancer drugs with MDR inhibitors as ligands for anticancer therapy.

Experimental Section

Synthesis and Chemical Characterization. [$RuCl_2$(η^6-*p*-cymene)]$_2$,[44] **3**,[33] and **4**[33] were synthesized following literature protocols. All other reagents and solvents were obtained from commercial sources and used without further purification. ^{1}H and ^{13}C NMR spectra were recorded on a Bruker 400 MHz spectrometer at rt in $CDCl_3$. The NMR spectra were referenced to internal solvents as follows: δ ($CHCl_3$, ^{1}H) = 7.26 and δ ($CDCl_3$, ^{13}C) = 77.00.[45] UV spectra were recorded on a Perkin-Elmer Lambda 900 spectrometer. Fluorescence measurements were carried out on a Jobin Yvon Fluorolog spectrometer. Electrospray ionization mass spectra (ESI-MS) were recorded on a Thermofinigan LCQ Deca

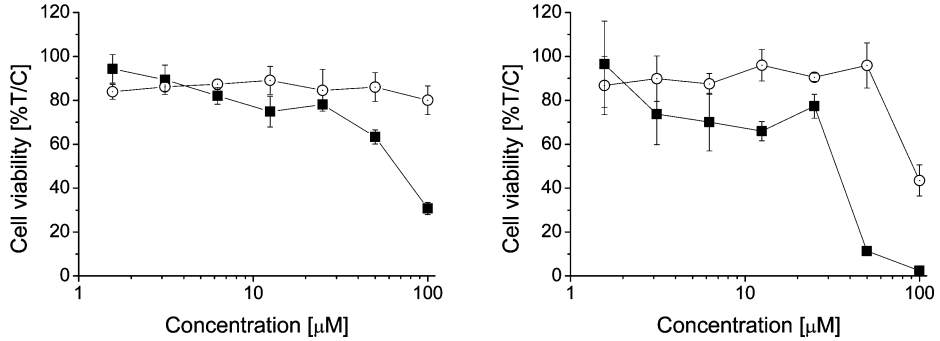

Figure 7. Comparison of cell viability by Alamar Blue (○) and ^{3}H-thymidine (■) assays after an exposure period of 6 h (left) and 8 h (right) to complex **10** on A549 lung carcinoma cells.

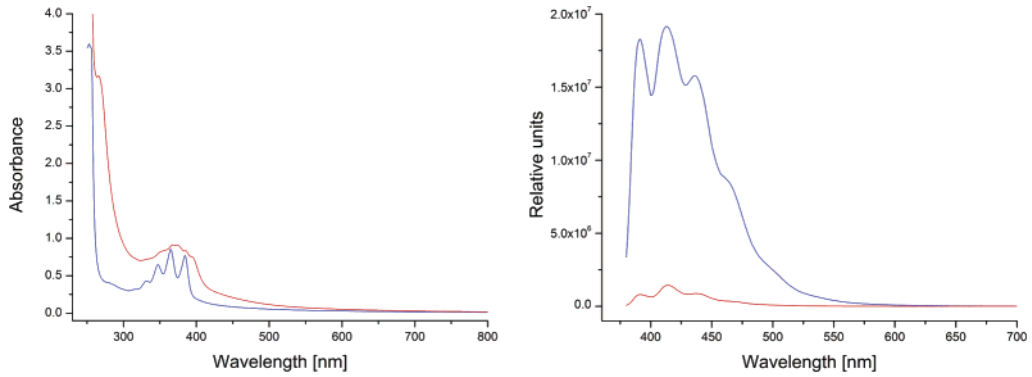

Figure 8. UV/vis absorption (left) and fluorescence emission (right) spectra for compounds **7** (blue) and **10** (red). For the fluorescence spectra, an irradiation wavelength of 365 nm was applied, according to the most intensive UV absorption band. The measurements were carried out under similar conditions as those used in the cell tests, with a substance concentration of 100 μM in 0.15 M aqueous NaCl solution containing 0.5% DMSO.

XP Plus quadrupole ion trap instrument in positive mode in CH_3CN, MeOH, or MeOH/0.1% HCOOH following a literature procedure.[46] Elementary analyses were provided by the analytical service of the EPFL.

2-(Imidazol-1-yl)-1-(phenoxazin-10-yl)-ethanone (Phenoximid; 5). To a solution of **3** (400 mg, 1.54 mmol) in CH_3CN (60 mL), KI (600 mg, 3.61 mmol, 2.35 equiv) and imidazole (420 mg, 6.17 mmol, 4.01 equiv) were added at rt. The resulting mixture was heated to reflux for 1 h. After cooling, the reaction mixture was diluted with H_2O (100 mL) and extracted with Et_2O (2 × 50 mL) and EtOAc (2 × 50 mL). The combined organic extracts were washed with brine (50 mL), dried over Na_2SO_4, and evaporated in vacuo. The crude product was purified by column chromatography (20 g SiO_2; CH_2Cl_2/NEt_3 50:1 → CH_2Cl_2/NEt_3 10:1), affording an off-white solid (353 mg, 1.21 mmol, 79%). ^{1}H NMR (400 MHz, $CDCl_3$): δ 5.01 (s, 2 H, 2-H_2), 6.93 (br s, 1 H, 5′-H), 7.07 (br s, 1 H, 4′-H), 7.16−7.22 (m, 2 H, 3″-H, 7″-H), 7.19 (d, J = 7.8 Hz, 2 H, 1″-H, 9″-H), 7.25−7.31 (m, 2 H, 2″-H, 8″-H), 7.44 (s, 1 H, 2′-H), 7.49 (d, J = 7.6 Hz, 2 H, 4″-H, 6″-H). ^{13}C NMR (100 MHz, $CDCl_3$): δ 48.49 (C-2), 117.4 (C-1″, C-9″), 120.0 (C-5′), 123.8 (C-3″, C-7″), 124.6 (C-4″, C-6″), 127.9 (C-2″, C-8″), 128.1 (C-9a″, C-10a″), 129.6 (C-4′), 138.0 (C-2′), 151.1 (C-4a″, C-5a″), 165.5 (C-1). ESI-MS (MeOH/0.1% HCOOH): m/z (%) 873.1 (55) [3M + H]$^+$, 582.6 (100) [2M + H]$^+$, 292.1 (72) [M + H]$^+$. Anal. ($C_{17}H_{13}N_3O_2$·0.33H_2O) C, H, N.

2-(Benzimidazol-1-yl)-1-(phenoxazin-10-yl)-ethanone (Phenoxbenzimid; 6). To a solution of **3** (400 mg, 1.54 mmol) in CH_3CN (60 mL), KI (600 mg, 3.61 mmol, 2.35 equiv) and benzimidazole (730 mg, 6.17 mmol, 4.01 equiv) were added at rt. The resulting mixture was heated to reflux for 1 h. After cooling, the reaction mixture was diluted with H_2O (100 mL) and extracted with EtOAc (2 × 50 mL). The combined organic extracts were washed with brine (25 mL), dried over Na_2SO_4, and evaporated in vacuo. The crude product was purified by column chromatography (40 g SiO_2; EtOAc/hexane 1:1 → EtOAc/EtOH 10:1), affording an off-white solid (200 mg, 0.586 mmol, 38%). ^{1}H NMR (400 MHz, $CDCl_3$): δ 5.22 (s, 2 H, 2-H_2), 7.16−7.23 (m, 5 H, 4′-H, 1″-H, 3″-H, 7″-H, 9″-H), 7.23−7.32 (m, 4 H, 5′-H, 6′-H, 2″-H, 8″-H), 7.54 (d, J = 7.9 Hz, 2 H, 4″-H, 6″-H), 7.75−7.81 (m, 1 H, 7′-H), 7.86 (br s, 1 H, 2′-H). ^{13}C NMR (100 MHz, $CDCl_3$): δ 46.46 (C-2), 109.1 (C-4′), 117.5 (C-1″, C-9″), 120.5 (C-7′), 122.4, 123.3 (C-5′, C-6′), 123.8 (C-3″, C-7″), 124.6 (C-4″, C-6″), 127.9 (C-2″, C-8″), 128.1 (C-9a″, C-10a″), 133.9 (C-7a′), 143.5 (C-3a′), 143.6 (C-2′), 151.1 (C-4a″, C-5a″), 165.3 (C-1). ESI-MS (MeOH/0.1% HCOOH): m/z (%) 873.1 (55) [3M + H]$^+$, 582.6 (100) [2M + H]$^+$, 292.1 (72) [M + H]$^+$. Anal. ($C_{21}H_{15}N_3O_2$·0.5H_2O) C, H, N.

***N*-(Anthracen-9-yl)-imidazole (anthraimid; 7).** A suspension of 9-bromoanthracene (2.57 g, 10.0 mmol), K_2CO_3 (3.46 g, 25.0 mmol, 2.50 equiv), imidazole (817 mg, 12.0 mmol, 1.20 equiv), CuI (50.6 mg, 0.266 mmol, 2.66 mol %) and L-proline (115 mg, 0.999 mmol, 10.0 mol %) in DMSO (20 mL) was degassed thoroughly. Next, the mixture was heated to 120 °C for 12 h. After cooling to rt overnight, the reaction mixture was partitioned between EtOAc (150 mL) and H_2O (150 mL). The aqueous layer was separated and extracted with EtOAc (2 × 50 mL). The combined organic layers were washed with brine (3 × 50 mL). From the collected brine washings, an additional organic layer separated. The combined organic layers were dried over Na_2SO_4. Silica gel (10 g) was added, and the solvent was removed in vacuo. Purification via gradient column chromatography (100 g silica gel; CH_2Cl_2 → CH_2Cl_2/EtOAc 3:1 → CH_2Cl_2/EtOAc 1:1 → CH_2Cl_2/EtOAc 1:3 → EtOAc) yielded the desired imidazole derivative as a yellow-brown solid (692 mg, 2.83 mmol, 28%). ^{1}H NMR (400 MHz, $CDCl_3$): δ 7.28 (s, 1 H, 5-H), 7.45 (s, 1 H, 4-H), 7.46 (d, J = 8.0 Hz, 2 H, 1′-H, 8′-H), 7.47−7.56 (m, 4 H, 2′-H, 3′-H, 6′-H, 7′-H), 7.79 (s, 1 H, 2-H), 8.09 (d, J = 8.0 Hz, 2 H, 4′-H, 5′-H), 8.61 (s, 1 H, 10′-H). ^{13}C NMR (100 MHz, $CDCl_3$): δ 122.4 (C-1′, C-8′), 122.7 (C-5), 125.9 (C-2′, C-7′), 127.6 (C-3′, C-6′), 128.4 (C-4′, C-5′), 128.5 (C-10′), 128.8 (C-4a′, C-10a′), 129.7 (C-4), 131.2 (C-8a′, C-9a′), 139.6 (C-2); signal for C-9′ not detectable. ESI-MS (MeOH/0.1% HCOOH): m/z (%) 245.7 (100) [M + H]$^+$. Anal. ($C_{17}H_{12}N_2$·0.2H_2O) C, H, N.

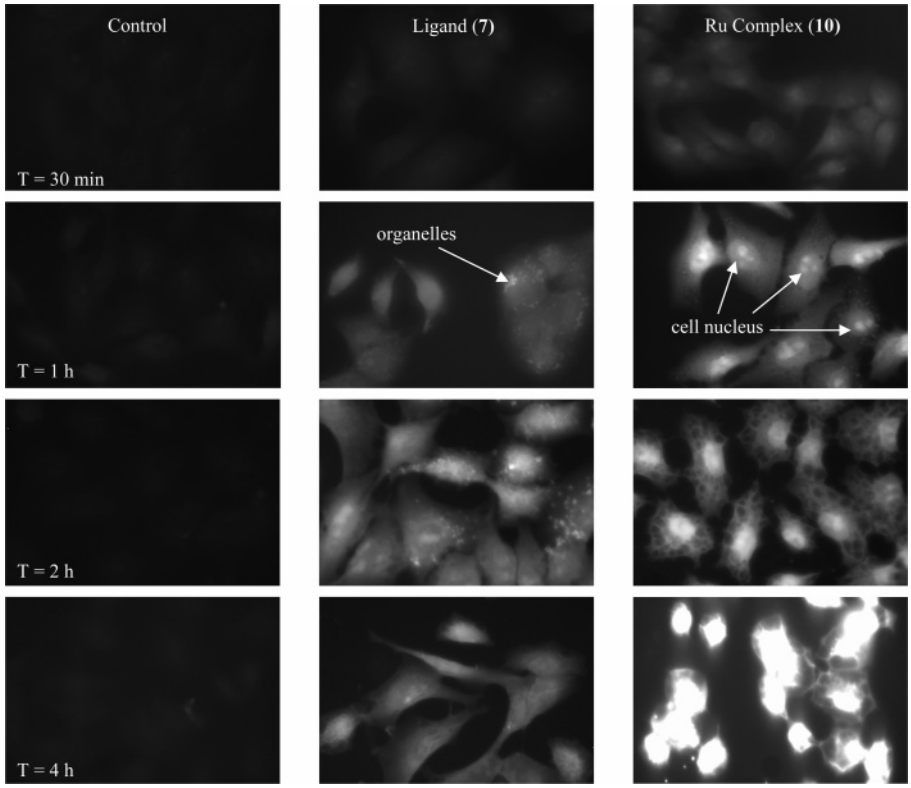

Figure 9. Fluoroscence microscopy photographs of A549 lung carcinoma cells exposed to the anthracene-imidazole ligand **7** (middle column) and the ruthenium−anthracene complex **10** (right column) compared to control (left column) at 0.5, 1, 2, and 4 h time periods of drug exposure. Drugs were applied at a 100 μM concentration. Cells were irradiated at 365 nm, and the photographs were exposed for 1 s, after a delay of 30 s upon irradiation.

[Ru(η^6-*p*-cymene)Cl$_2$(phenoximid)] (8). To a solution of [Ru(η^6-*p*-cymene)Cl$_2$]$_2$ (60.0 mg, 98.0 μmol) in CH_2Cl_2 (10 mL), **5** (58.0 mg, 199 μmol, 2.03 equiv) was added at rt. The resulting mixture was stirred at rt for 1 h. The solvent was removed in vacuo. The residue was redissolved in CH_2Cl_2 (5 mL). Et_2O (80 mL) was added, and the mixture was allowed to stand at rt for 2 h. The precipitate was filtered, washed with Et_2O (3 × 10 mL), and dried in vacuo, affording an orange-yellow solid (45.7 mg, 76.5 μmol, 39%). ^{1}H NMR (400 MHz, $CDCl_3$): δ 1.28 (d, J = 6.9 Hz, 6 H, 1-CH(C*H*$_3$)$_2$), 2.13 (s, 3 H, 4-C*H*$_3$), 2.95 (sept, J = 6.9 Hz, 1 H, 1-C*H*(CH$_3$)$_2$), 4.90 (br s, 2 H, 1″-H$_2$), 5.26 (d, J = 6.0 Hz, 2 H, 2-H, 6-H), 5.46 (d, J = 6.0 Hz, 2 H, 3-H, 5-H), 6.80 (t, J = 1.5 Hz, 1 H, 4′-H), 7.15 (dd, J = 7.8, 1.7 Hz, 2 H, 1‴-H, 9‴-H), 7.16−7.27 (m, 5 H, 5′-H, 2‴-H, 3‴-H, 7‴-H, 8‴-H), 7.49 (dd, J = 7.7, 1.4 Hz, 2 H, 4‴-H, 6‴-H), 7.99 (br s, 1 H, 2′-H). ^{13}C NMR (100 MHz, $CDCl_3$): δ 18.47 (4-*C*H$_3$), 22.30 (1-CH(*C*H$_3$)$_2$), 30.66 (1-*C*H(CH$_3$)$_2$), 49.23 (C-1″), 81.27 (C-2, C-6), 82.83 (C-3, C-5), 97.37 (C-4), 102.6 (C-1), 117.3 (C-1″, C-9″), 121.1 (C-4′), 124.0 (C-3‴, C-7‴), 124.9 (C-4‴, C-6‴), 127.8 (C-9a‴, C-10a‴), 127.8 (C-2‴, C-8‴), 131.3 (C-5′), 141.2 (C-2′), 151.0 (C-4a‴, C-5a‴), 165.1 (C-2″). ESI-MS (CH_3CN): *m*/*z* (%) 852.7 (61) [Ru(cymene)Cl(phenoximid)$_2$]$^+$, 602.3 (100) [Ru(cymene)Cl(CH_3CN)(phenoximid)]$^+$, 562.0 (57) [Ru(cymene)Cl(phenoximid)]$^+$. Anal. ($C_{27}H_{27}Cl_2N_3O_2Ru\cdot 0.75H_2O$) C, H, N.

[Ru(η^6-*p*-cymene)Cl$_2$(phenoxbenzimid)]·CH$_2$Cl$_2$ (9). [Ru(η^6-*p*-cymene)Cl$_2$]$_2$ (60.0 mg, 98.0 μmol) and **6** (70.0 mg, 205 μmol, 2.09 equiv) were dissolved in CH_2Cl_2 (15 mL). The resulting mixture was stirred at rt for 3 h. Et_2O (40 mL) was added, and the mixture was allowed to stand at rt for 0.5 h. The precipitate was filtered, washed with Et_2O (2 × 5 mL), and dried in vacuo, affording an intensive orange-yellow solid (122 mg, 167 μmol, 85%). Crystals suitable for X-ray analysis with EtOAc included as solvate were grown from CH_2Cl_2/EtOAc by slow evaporation at rt. ^{1}H NMR (400 MHz, $CDCl_3$): δ 1.30 (d, J = 6.9 Hz, 6 H, 1-CH(C*H*$_3$)$_2$), 2.01 (s, 3 H, 4-C*H*$_3$), 2.96 (sept, J = 6.9 Hz, 1 H, 1-C*H*(CH$_3$)$_2$), 5.01 (br s, 2 H, 1″-H$_2$), 5.34 (d, J = 5.8 Hz, 2 H, 2-H, 6-H), 5.58 (d, J = 5.8 Hz, 2 H, 3-H, 5-H), 7.05 (d, J = 7.4 Hz, 1 H, 7′-H), 7.17−7.24 (m, 6 H, 5′-H, 6′-H, 3‴-H, 4‴-H, 6‴-H, 7‴-H), 7.24−7.31 (m, 2 H, 2‴-H, 8‴-H), 7.55 (d, J = 7.7 Hz, 2 H, 4‴-H, 6‴-H), 8.02 (d, J = 7.3 Hz, 1 H, 4′-H), 8.40 (br s, 1 H, 2′-H). ^{13}C NMR (100 MHz, $CDCl_3$): δ 18.41 (4-CH$_3$), 22.42 (1-CH(*C*H$_3$)$_2$), 30.63 (1-*C*H(CH$_3$)$_2$), 46.67 (C-1″), 80.86 (C-2, C-6), 83.34 (C-3, C-5), 97.72 (C-4), 102.8 (C-1), 110.7 (C-7′), 117.4 (C-1‴, C-9‴), 120.3 (C-4′), 123.4 (C-3‴, C-7‴), 123.9, 124.5 (C-5′, C-6′), 125.0 (C-4‴, C-6‴), 127.9 (C-2‴, C-8‴, C-9a‴, C-10a‴), 133.9 (C-3a′), 143.2 (C-7a′), 146.2 (C-2′), 151.0 (C-4a‴, C-5a‴), 164.8 (C-2″). ESI-MS (CH_3CN): *m*/*z* (%) 952.7 (15) [Ru(cymene)Cl(phenoxbenzimid)$_2$]$^+$, 652.3 (58) [Ru(cymene)Cl(CH_3CN)(phenoxbenzimid)]$^+$, 612.0 (100) [Ru(cymene)Cl(phenoxbenzimid)]$^+$, 311.8 (40) [Ru(cymene)Cl(CH_3CN)]$^+$. Anal. ($C_{31}H_{29}Cl_2N_3O_2Ru\cdot CH_2Cl_2\cdot 0.25H_2O$) C, H, N.

[Ru(η^6-*p*-cymene)Cl$_2$(anthraimid)] (10). To a solution of [Ru(η^6-*p*-cymene)Cl$_2$]$_2$ (75.0 mg, 0.122 mmol) in CH_2Cl_2 (10 mL), **7** (60.0 mg, 0.246 mmol, 2.01 equiv) was added at rt. The resulting mixture was stirred at rt for 3 h. Subsequently, EtOAc (10 mL) and petrol ether (40 mL) were added, and the resulting suspension was stirred at rt for 3 min. The precipitate was filtered, washed with petrol ether (2 × 5 mL), and dried in vacuo, affording an orange solid (95.7 mg, 0.174 mmol, 71%). Crystals suitable for X-ray analysis were grown from CH_2Cl_2/EtOAc by slow evaporation at rt. ^{1}H NMR (400 MHz, $CDCl_3$): δ 1.36 (d, J = 6.9 Hz, 6 H, 1-CH(C*H*$_3$)$_2$), 2.29 (s, 3 H, 4-C*H*$_3$), 3.07 (sept, J = 6.9 Hz, 1 H, 1-C*H*(CH$_3$)$_2$), 5.35 (d, J = 6.0 Hz, 2 H, 2-H, 6-H), 5.56 (d, J = 6.0 Hz, 2 H, 3-H, 5-H), 7.24 (t, J = 1.4 Hz, 1 H, 4′-H), 7.39−7.44 (m, 2 H, 1″-H, 8″-H), 7.49−7.57 (m, 4 H, 2″-H, 3″-H, 6″-H, 7″-H), 7.75 (t, J = 1.4 Hz, 1 H, 5′-H), 8.05−8.12 (m, 2 H, 4″-H, 5″-H), 8.25 (t, J = 1.4 Hz, 1 H, 2′-H), 8.63 (s, 1 H, 10″-H). ^{13}C NMR (100 MHz, $CDCl_3$): δ 18.68 (4-*C*H$_3$), 22.36 (1-CH(*C*H$_3$)$_2$), 30.85 (1-*C*H(CH$_3$)$_2$), 81.36 (C-2, C-6), 83.01 (C-3, C-5), 97.55 (C-4), 102.5 (C-1), 121.8 (C-1″, C-8″), 123.1 (C-4′), 126.0 (C-2″, C-7″), 128.3 (C-3″, C-6″, C-4a″, C-10a″), 128.5 (C-4″, C-5″), 129.4 (C-10″), 131.1 (C-8a″, C-9a″), 132.3 (C-5′), 142.4 (C-2′); signal for C-9″ not detectable. ESI-MS (CH_3CN): *m*/*z* (%) 758.9 (20) [Ru(cymene)Cl(anthraimid)$_2$]$^+$, 556.2 (51) [Ru(cymene)Cl-

(CH_3CN)(anthraimid)]$^+$, 515.8 (100) [Ru(cymene)Cl(anthraimid)]$^+$, 312.1 (13) [Ru(cymene)Cl(CH_3CN)]$^+$. Anal. ($C_{27}H_{26}Cl_2N_2Ru\cdot 0.125H_2O$) C, H, N.

[Ru(η^6-*p*-cymene)Cl(phenoximid)$_2$][BPh$_4$] (11). To a solution of [Ru(η^6-*p*-cymene)Cl$_2$]$_2$ (40.0 mg, 65.3 μmol) in MeOH (20 mL), **5** (77.0 mg, 264 μmol, 4.05 equiv) was added at rt. The resulting mixture was stirred at rt for 10 min. NaBPh$_4$ (45.0 mg, 131 μmol, 2.01 equiv) was added and immediately a yellow precipitate formed. The mixture was stirred at rt for 3 h. The precipitate was filtered, washed with MeOH (6 mL), and dried in vacuo, affording a yellow solid (45.2 mg, 38.5 μmol, 29%). The filtrate was evaporated in vacuo. The yellow solid was washed with MeOH (5 mL) and dried in vacuo, affording a second fraction of product (66.3 mg, 56.5 μmol, 43%). ^{1}H NMR (400 MHz, $CDCl_3$): δ 1.16 (d, $J = 6.9$ Hz, 6 H, 1-CH(CH_3)$_2$), 1.82 (s, 3 H, 4-CH_3), 2.61 (sept, $J = 6.9$ Hz, 1 H, 1-CH(CH$_3$)$_2$), 4.16 (br d, $J_{AB} = 17.4$ Hz, 2 H, 2 × 1″-H$_A$), 4.26 (br d, $J_{AB} = 17.4$ Hz, 2 H, 2 × 1″-H$_B$), 5.18 (d, $J = 6.0$ Hz, 2 H, 2-H, 6-H), 5.54 (d, $J = 6.0$ Hz, 2 H, 3-H, 5-H), 6.32 (br s, 2 H, 2 × 4′-H), 6.87 (br t, $J = 7.1$ Hz, 4 H, 4 × *para*-H {BPh$_4$}), 6.94 (t, $J = 7.1$ Hz, 8 H, 8 × *meta*-H {BPh$_4$}), 7.03 (br s, 2 H, 2 × 5′-H), 7.06−7.25 (m, 16 H, 2 × 1‴-H, 2 × 2‴-H, 2 × 3‴-H, 2 × 4‴-H, 2 × 5‴-H, 2 × 6‴-H, 2 × 7‴-H, 2 × 8‴-H), 7.37−7.42 (br. m, 10 H, 8 × *ortho*-H {BPh$_4$}, 2 × 2′-H). ^{13}C NMR (100 MHz, $CDCl_3$): δ 18.16 (4-*C*H$_3$), 22.38 (1-CH(*C*H$_3$)$_2$), 30.75 (1-*C*H(CH$_3$)$_2$), 49.25 (2 × C-1″), 80.69 (C-2, C-6), 86.60 (C-3, C-5), 100.6 (C-4), 102.8 (C-1), 117.3 (2 × C-1‴, 2 × C-9‴), 122.1 (4 × *para*-C {BPh$_4$}), 122.2 (2 × C-4′), 124.0 (2 × C-3‴, 2 × C-7‴), 124.7 (2 × C-4‴, 2 × C-6‴), 125.8 (q, $J_{CB} = 2.6$ Hz, 8 × *meta*-C {BPh$_4$}), 127.6 (2 × 9a‴, 2 × 10a‴), 127.9 (2 × C-2‴, 2 × C-8‴), 130.2 (2 × C-5′), 136.1 (q, $J_{CB} = 1.4$ Hz, 8 × *ortho*-C {BPh$_4$}), 140.9 (2 × C-2′), 150.9 (2 × C-4a‴, 2 × C-5a‴), 164.0 (q, $J_{CB} = 49.2$ Hz, 4 × *ipso*-C {BPh$_4$}), 164.7 (2 × C-2″). **ESI-MS** (CH_3CN): *m*/*z* (%) = 852.7 (100) [Ru(cymene)Cl(phenox-imid)$_2$]$^+$. **Anal.** ($C_{68}H_{60}BClN_6O_4Ru\cdot 0.66\ H_2O$) C, H, N.

[Ru(η^6-*p*-cymene)Cl(anthraimid)$_2$][BPh$_4$] (12). To a solution of [Ru(η^6-*p*-cymene)Cl$_2$]$_2$ (50.0 mg, 81.6 μmol) in MeOH (40 mL), **7** (80.0 mg, 327 μmol, 4.01 equiv), and NaBPh$_4$ (56.0 mg, 164 μmol, 2.01 equiv) were added at rt. The resulting mixture was heated to reflux for 3 h. After cooling, the formed precipitate was filtered, washed with MeOH (5 mL) and pentane (2 × 5 mL), and dried in vacuo, affording a bright yellow solid (90.4 mg, 83.8 μmol, 51%). Crystals suitable for X-ray analysis were grown from CH_2Cl_2/EtOAc by slow evaporation at rt. ^{1}H NMR (400 MHz, $CDCl_3$): δ 1.29 (d, $J = 6.9$ Hz, 6 H, 1-CH(CH_3)$_2$), 1.88 (s, 3 H, 4-CH_3), 2.68 (sept, $J = 6.9$ Hz, 1 H, 1-CH(CH$_3$)$_2$), 5.04 (d, $J = 6.0$ Hz, 2 H, 2-H, 6-H), 5.45 (d, $J = 6.0$ Hz, 2 H, 3-H, 5-H), 6.74 (br t, $J = 7.2$ Hz, 4 H, 4 × *para*-H {BPh$_4$}), 6.94 (t, $J = 7.3$ Hz, 8 H, 8 × *meta*-H {BPh$_4$}), 6.95 (d, $J = 7.7$ Hz, 2 H, 2 × 1″-H), 7.14 (d, $J = 8.0$ Hz, 2 H, 2 × 8″-H), 7.20 (t, $J = 7.7$ Hz, 2 H, 2 × 2″-H), 7.21 (br s, 2 H, 2 × 4′-H), 7.26 (br s, 2 H, 2 × 5′-H), 7.40−7.46 (br m, 10 H, 2 × 7″-H, 8 × *ortho*-H {BPh$_4$}), 7.49 (t, $J = 7.7$ Hz, 2 H, 2 × 3″-H), 7.56 (t, $J = 8.0$ Hz, 2 H, 2 × 6″-H), 7.95 (br s, 2 H, 2 × 2′-H), 8.11 (d, $J = 7.7$ Hz, 2 H, 2 × 4″-H), 8.14 (d, $J = 8.0$ Hz, 2 H, 2 × 5″-H), 8.69 (s, 2 H, 2 × 10″-H). ^{13}C NMR (100 MHz, $CDCl_3$): δ 18.38 (4-*C*H$_3$), 22.49 (1-CH(*C*H$_3$)$_2$), 31.10 (1-*C*H(CH$_3$)$_2$), 80.95 (C-2, C-6), 86.89 (C-3, C-5), 100.2 (C-4), 102.3 (C-1), 120.7, 120.8 (C-1″, C-8″), 121.9 (4 × *para*-C {BPh$_4$}), 124.6 (2 × C-4′), 125.7 (q, $J_{CB} = 2.7$ Hz, 8 × *meta*-C {BPh$_4$}), 126.1, 126.2 (C-2″, C-7″), 128.1, 128.2 (2 × C-4a″, 2 × C-10a″), 128.6, 128.6 (2 × C-3″, 2 × C-6″), 128.8, 128.9 (2 × C-4″, 2 × C-5″), 130.0 (2 × C-10″), 131.0, 131.1 (2 × C-8a″, 2 × C-9a″), 132.2 (2 × C-5′), 134.5 (2 × C-9″), 136.3 (q, $J_{CB} = 1.5$ Hz, 8 × *ortho*-C {BPh$_4$}), 141.4 (2 × C-2′), 164.1 (q, $J_{CB} = 49.3$ Hz, 4 × *ipso*-C {BPh$_4$}). ESI-MS (MeOH): *m*/*z* (%) 758.9 (100) [Ru(cymene)Cl(anthraimid)$_2$]$^+$, 515.1 (8) [Ru(cymene)Cl(anthraimid)]$^+$. Anal. ($C_{68}H_{58}BClN_4Ru\cdot 0.5H_2O$) C, H, N.

UV/Vis and Fluorescence Measurements. The solutions for UV/vis and fluorescence measurements were prepared by dissolving 12.5 μL of a 20 mM stock solution of compounds **7** and **10** in DMSO in 2.5 mL of 0.15 M aqueous NaCl solution. The obtained samples had the following specifications: 100 μM compound, 0.15 M NaCl, and 0.5% DMSO. A 0.5% solution of DMSO in 0.15 M aqueous NaCl was used as comparative standard.

In Vitro Tests. Cells and Cell Culture Conditions. TS/A murine adenocarcinoma cell line, initially obtained from Dr. G. Forni (CNR, Centro di Immunogenetica ed Oncologia Sperimentale, Torino, Italy), were maintained in RPMI-1640 medium (EuroClone, Wetherby, U.K.) supplemented with 10% fetal bovine serum (FBS, Invitrogen, Milano, Italy), 2 mM L-glutamine (EuroClone, Wetherby, U.K.), and 50 μg/mL gentamycin sulfate solution (EuroClone, Wetherby, U.K.).

HBL-100, a nontumorigenic human breast cell line was obtained from the American Type Culture Collection (ATCC, Manassas, VA) and was maintained in McCoy's 5A medium (Sigma, St. Louis, MO), supplemented with 10% FBS, 2 mM L-glutamine, 100 UI/mL penicillin, and 100 μg/mL streptomycin (EuroClone, Whetherby, U.K.),

Human T47D breast carcinoma, A549 lung carcinoma, and HT-29 colon carcinoma cell lines were from the ATCC. All other cell culture reagents were obtained from Gibco-BRL, Basel, Switzerland. The cells were routinely grown in DMEM medium containing 4.5 g/L glucose, 10% foetal calf serum, and antibiotics.

For evaluation of ruthenium compounds, cells were grown in multiwell cell culture plastic plates (Corning Costar Italia) for 24 h then exposed for 24, 48, or 72 h to the appropriate compound at a concentration of 1−300 μM. Solutions of the substances for application were prepared by diluting a freshly prepared stock solution of the corresponding compound in DMSO (20 mM for A549, HT29, T47D; 10 mM for TS/A, HBL-100) with the appropiate medium for the cell line (see above) containing 5% of serum. Maximum DMSO concentration in the cells was 0.5% v/v (A549, HT29, T47D) and 1% v/v (TS/A, HBL-100). Analysis of cell viability and growth was performed at the end of the incubation time.

Evaluation of Cell Growth. Cell mitochondrial functions were determined by the MTT test, essentially as previously described,[47] survival was determined by the Alamar Blue test (as described below), and DNA synthesis by the incorporation of thymidine, as previously described.[48] Briefly, MTT [3-(4,5-dimethylthiazol-2-yl)-2,5-diphenyltetrazolium bromide, Sigma, Switzerland, dissolved in PBS (5 mg/mL) was added (2.5 μL per 100 μL of medium) to all wells, and the plates were incubated at 37 °C for 2 h, then the precipitated formazan was dissolved in DMSO, and optical density was measured at 570 nm on a SpectraCount Packard (Meriden, CT) instrument. To assess DNA synthesis, 1 μCi/mL ^{3}[H]-thymidine (Amersham Pharmacia, Dübendorf, Switzerland), was added for the last 2 h of exposure to compounds and incorporation was quantified in a beta-counter (Rackbeta, LKB) after precipitation with 10% trichloracetic acid and solubilization in 0.1 N NaOH + 1% SDS.

Alamar Blue reduction was used to quantify metabolically active cells. Briefly, following treatment, cells were exposed to 10% Alamar Blue (Serotec, Düsseldorf, Germany) and added to the cell culture medium without medium change for 2 h, then fluorescence increase was recorded for 30 min at 37 °C in a thermostated multiwell fluorescence reader (Cytofluor, PerSeptive BioSystems) at $\lambda_{ex}/\lambda_{em} = 530$ nm/580 nm.

Calcein Uptake Assay. The Pgp activity of A549 lung carcinoma was evaluated by calcein-AM uptake assay in the method described by Weiss et al.[37] The assay was performed on cells seeded in 48-well plates. Prior to the assay, the cells were washed twice with pre-warmed Hanks balanced salt solution, supplemented with 10 mM HEPES (HHBSS) and preincubated with HHBSS for 30 min and then with the drug for 15 min. Calcein-AM (Fluka), predissolved in dry DMSO, was then added (to reach a final concentration of 1 μM), and the cells were incubated for an additional 60 min. The uptake was stopped by transferring the plates onto ice, and the cells were washed twice with chilled HHBSS. The cells were then lysed in 1% Triton X-100/PBS for 15 min, and the fluorescence of the calcein generated was analyzed in a multiwell fluorometric

plate reader, λ_{ex} = 485 nm excitation and λ_{em} = 530 filters (PerSeptive, Biosystems, MA).

Visualization of Cell Drug Uptake by Fluorescence Microscopy. A549 lung carcinoma cells grown on microscope slides were exposed to compounds **7** and **10** for 0.5−4 h. The medium was aspirated, and the cell slides were washed twice with PBS, fixed in 4% buffered paraformaldehyde for 5 min, and washed twice with PBS. For visualization, the cell slides were irradiated at 365 nm using an Axioplan 2 imaging fluorescence microscope (Zeiss, Germany). Images were taken using an Axiocam MRm camera (Zeiss, Germany) with an exposure time of 1000 ms.

Crystallography. Suitable single crystals were removed from the sample vial and manipulated in a grease matrix. The crystals were mounted to the end of a glass capillary (diameter 0.1 mm) attached to a metal pin affixed to a goniometer head, which was placed in the cradle. For structures **9** and **12**, a Burker−Nonius KappaCDD diffractometer equipped with an Apex II CCD area detector and an Enraf-Nonius FR590 X-ray generator was used, while for **10**, an Oxford-Kuma Xcalibur diffractor with a Sapphire CCD area detector was employed. Both instruments utilize a graphite-monochromotated Mo K_α radiation source with λ = 0.710 73 Å. The crystal was kept under a −133 or −173 °C gaseous flow of N_2 during the collection procedure. The unit cell and orientation matrix were determined by indexing reflections measured from a sampling scan and analyzed with either the program DIRAX[49] or, in the case of **10**, strong reflections from the entire data collection were used and processed with CrysAlis RED.[50] All data collections were performed by scanning reflections from the entire Ewald sphere using the programs CollectCCD[51] and CrysAlis CCD.[50] After data integration with either EvalCCD[51] or CrysAlis RED,[50] a multiscan absorption correction based on a semiempirical method was applied using the SADABS[52] or Multiscan[53] program. Space group determination was performed with the XPREP[54] program. A structure solution based on the direct-method algorithm was employed with the program SHELXS.[55] Afterward, anisotropic refinement of all non-hydrogen atoms was completed based on a least-squares full-matrix method against F^2 data using SHELXL.[55] Hydrogen atoms were added through geometrical calculated positions and refined as a riding model using a scaled thermal parameter of the connecting atom. In structure **9**, the thermal parameters of two carbon atoms, C3 and C5, were isotropically restrained with an esd of 0.01. A small number of reflections in structure **10** were removed when $\Delta(F_o^2 - F_c^2)$/esd exceeded 10.0. Graphical representations of the structures were made with ORTEP-3.[56] Important data for all structures is given in the SI. Other specific crystallographic details are provided in the accompanying CIF files.

Acknowledgment. We thank the Swiss Cancer League, the EPFL, COST (Switzerland), LINFA laboratories, and MADE, a project funded by CRTrieste Foundation, for support. We also thank Romain Despland for practical synthetic assistance and Frédéric Gumy, Dr. Helen Mary O'Hare, and Dr. Annina Aebischer for help with the UV and fluorescence measurements. A postdoc stipend provided from the German Academic Exchange Service (DAAD) and the Swiss National Science Foundation (SNF) for C.A.V. is gratefully acknowledged.

Supporting Information Available: Crystallographic data for compounds **9**, **10**, and **12** in CIF format, the structures of amiodarone, fluphenazine, and cyclosporine A, structures for all synthesized compounds with numbering schemes for NMR assignments, and crystallographic tables.. This material is available free of charge via the Internet at http://pubs.acs.org.

References

(1) Teodori, E.; Dei, S.; Scapecchi, S.; Gualtieri, F. The medicinal chemistry of multidrug resistance (MDR) reversing drugs. *Farmaco* **2002**, *57*, 385−415.
(2) Hill, B. Drug resistance: An overview of the current state of the art. *Int. J. Oncol.* **1996**, *9*, 197−203.
(3) Lacombe, P. S.; Vicente, J. A. G.; Pagès, J. G.; Morselli, P. L. Causes and problems of nonresponse or poor response to drugs. *Drugs* **1996**, *51*, 552−570.
(4) Endicott, J. A.; Ling, V. The biochemistry of P-glycoprotein-mediated multidrug resistance. *Annu. Rev. Biochem.* **1989**, *58*, 137−171.
(5) Mitscher, L. A.; Pillai, S. P.; Gentry, E. J.; Shankel, D. M. Multiple drug resistance. *Med. Res. Rev.* **1999**, *19*, 477−496.
(6) Volm, M.; Mattern, J. Resistance mechanisms and their regulation in lung cancer. *Crit. Rev. Oncog.* **1996**, *7*, 227−244.
(7) Gately, D. P.; Howell, S. B. Cellular accumulation of the anticancer agent cisplatin−A review. *Brit. J. Cancer* **1993**, *67*, 1171−1176.
(8) Dietel, M. What's new in cytostatic drug resistance and pathology. *Pathol., Res. Pract.* **1991**, *187*, 892−905.
(9) Hammond, J. R.; Johnstone, R. M.; Gros, P. Enhanced efflux of (3H)-vinblastine from Chinese hamster ovary cells transfected with a full-length complementary DNA clone for the mdr 1 gene. *Cancer Res.* **1989**, *49*, 3867−3871.
(10) Morrow, C. S.; Cowan, K. H. Glutathione S-transferases and drug resistance. *Cancer Cells* **1990**, *2*, 15−22.
(11) Kessel, D.; Bottenrill, V.; Wodinsky, I. Uptake and retention of daunomycin by mouse leukemic cells as factors in drug response. *Cancer Res.* **1968**, *28*, 938−941.
(12) Aszalos, A.; Ross, D. D. Biochemical and clinical aspects of efflux pump related resistance to anti-cancer drugs. *Anticancer Res.* **1998**, *18*, 2937−2944.
(13) Renes, J.; De Vries, E. G. E.; Nienhuis, E. F.; Jansen, P. L. M.; Muller, M. ATP- and glutathione-dependent transport of chemotherapeutic drugs by the multidrug resistance protein MRP1. *Br. J. Pharmacol.* **1999**, *126*, 681−688.
(14) Rappa, G.; Lorico, A.; Flavell, R. A.; Sartorelli, A. C. Evidence that the multidrug resistance protein (MRP) functions as a co-transporter of glutathione and natural product toxins. *Cancer Res.* **1997**, *57*, 5232−5237.
(15) Manciu, L.; Chang, X.-B.; Riordan, J. R.; Ruysschaert, J. M. Multidrug resistance protein MRP1 reconstituted into lipid vesicles: Secondary structure and nucleotide-induced tertiary structure changes. *Biochemistry* **2000**, *39*, 13026−13033.
(16) Croop, J. M. Evolutionary relationships among ABC transporters. *Methods Enzymol.* **1998**, *292*, 101−116.
(17) Dey, S.; Ramachandra, M.; Pastan, I.; Gottesman, M. M.; Ambudkar, S. V. Photoaffinity labeling of human P-glycoprotein: Effect of modulator interaction and ATP hydrolysis on substrate binding. *Methods Enzymol.* **1998**, *292*, 318−328.
(18) Abramson, R.; Bhushan, A.; Dolci, E.; Tritton, T. The structure of the multidrug resistance P-glycoprotein and its similarity to other proteins. *Ann. Rep. Med. Chem.* **1989**, *25*, 253−260.
(19) Wang, G.; Pincheira, R.; Zhang, J.-T. Dissection of drug-binding-induced conformational changes in P-glycoprotein. *Eur. J. Biochem.* **1998**, *255*, 383−390.
(20) Tsuruo, T.; Iida, H.; Tsukagoshi, S.; Sakurai, Y. Overcoming of vincristine resistance in P388 leukemia in vivo and in vitro through enhanced cytotoxicity of vincristine and vinblastine by verapamil. *Cancer Res.* **1981**, *41*, 1967−1972.
(21) Belpomme, D.; Gauthier, S.; Pujade-Lauraine, E.; Facchini, T.; Goudier, M.-J.; Krakowski, I.; Netter-Pinon, G.; Frenay, M.; Gousset, C.; Marie, F. N.; Benmiloud, M.; Sturz, F. Verapamil increases the survival of patients with anthracycline-resistant metastatic breast carcinoma. *Ann. Oncol.* **2000**, *11*, 1471−1476.
(22) Aird, R. E.; Cummings, J.; Ritchie, A. A.; Muir, M.; Morris, R. E.; Chen, H.; Sadler, P. J.; Jodrell, D. I. In vitro and in vivo activity and cross resistance profiles of novel ruthenium(II) organometallic arene complexes in human ovarian cancer. *Brit. J. Cancer* **2002**, *86*, 1652−1657.
(23) Haussermann, K.; Benz, B.; Gekeler, V.; Schumacher, K.; Eichelbaum, M. Effects of verapamil enantiomers and major metabolites on the cytotoxicity of vincristine and daunomycin in human lymphoma cells. *Eur. J. Clin. Pharmacol.* **1991**, *40*, 53−59.
(24) Bates, S. E.; Wilson, W. H.; Foio, A. T.; Alvarez, M.; Zhan, Z.; Regis, J.; Robey, R.; Hose, C.; Monks, A.; Kang, Y. K.; Chabner, B. Clinical reversal of multidrug resistance. *Stem Cells* **1996**, *14*, 56−63.
(25) Chauffert, B.; Rey, D.; Condert, B.; Durmas, M.; Martin, F. Amiodarone is more efficient than verapamil in reversing resistance to anthracyclines in tumor cells. *Br. J. Cancer* **1987**, *56*, 119−122.
(26) Hait, W. N.; Morris, S.; Lazo, J. S. Phase I trial of combined therapy with bleomycin and the calmodulin antagonist trifluoperazine. *Cancer Chemother. Pharmacol.* **1989**, *23*, 358−365.
(27) Slater, L. M.; Sweet, P.; Stupecky, M.; Gupta, S. Cyclosporin A reverses vincristine and daunorubicin resistance in acute lymphatic leukemia *in vitro*. *J. Clin. Invest.* **1996**, *77*, 1405−1412.

(28) Tsuruo, T.; Naito, M.; Tomida, A.; Fujita, N.; Mashima, T.; Sakamoto, H.; Haga, N. Molecular targeting therapy of cancer: Drug resistance, apoptosis and survival signal. *Cancer Sci.* **2003**, *94*, 1, 15−21.
(29) Dyson, P. J.; Sava, G. Metal-based antitumour drugs in the post genomic era. *Dalton Trans.* **2006**, 1929−1933.
(30) (a) Timerbaev, A. R.; Hartinger, C. G.; Aleksenko, S. S.; Keppler, B. K. Interactions of antitumor metallodrugs with serum proteins: Advances in characterization using modern analytical methodology. *Chem. Rev.* **2006**, *106*, 2224−2248. (b) Pongratz, M.; Schluga, P.; Jakupec, M. A.; Arion, V. B.; Hartinger, C. G.; Allmaier, G.; Keppler, B. K. Transferrin binding and transferrin-mediated cellular uptake of the ruthenium coordination compound KP1019, studied by means of AAS, ESI-MS and CD spectroscopy. *J. Anal. At. Spectrom.* **2004**, *19*, 46−51.
(31) Srivastava, S. C.; Richards P.; Meinken, G. E.; Larson, S. M.; Grunbaum, Z. In *Radiopharmaceuticals: Structure activity relationship*; Spencer, R. P., Ed.; Grune and Stratton: New York, 1981; pp 207−223.
(32) (a) Scolaro, C.; Geldbach, T. J.; Rochat, S.; Dorcier, A.; Gossens, C.; Bergamo, A.; Cocchietto, M.; Tavernelli, I.; Sava, G.; Rothlisberger, U.; Dyson, P. J. Influence of hydrogen-bonding substituents on the cytotoxicity of RAPTA compounds. *Organometallics* **2006**, *25*, 756−765. (b) Dorcier, A.; Dyson, P. J.; Gossens, C.; Rothlisberger, U.; Scopelliti, R.; Tavernelli, I. Binding of organometallic ruthenium(II) and osmium(II) complexes to an oligonucleotide: A combined mass spectrometric and theoretical study. *Organometallics* **2005**, *24*, 2114−2123. (c) Scolaro, C.; Bergamo, A.; Brescacin, L.; Delfino, R.; Cocchietto, M.; Laurenczy, G.; Geldbach, T. J.; Sava, G.; Dyson, P. J. In vitro and in vivo evaluation of ruthenium(II)−arene PTA complexes. *J. Med. Chem.* **2005**, *48*, 4161−4171. (d) Allardyce, C. S.; Dyson, P. J.; Ellis, D. J.; Heath, S. L. [Ru(η^6-*p*-cymene)Cl_2(pta)] (pta = 1,3,5-triaza-7-phosphatricyclo[3.3.1.1]-decane): A water soluble compound that exhibits pH dependent DNA binding providing selectivity for diseased cells. *Chem. Commun.* **2001**, 1396−1397.
(33) Thimmaiah, K. N.; Horton, J. K.; Seshadri, R.; Israel, M.; Houghton, J. A.; Harwood, F. C.; Houghton, P. J. Synthesis and chemical characterisation of *N*-substituted phenoxazines directed toward reversing vinca alkaloid resistance in multidrug-resistant cancer cells. *J. Med. Chem.* **1992**, *35*, 3358−3364.
(34) Vock, C. A.; Scolaro, C.; Phillips, A. D.; Scopelliti, R.; Sava, G.; Dyson, P. J. Synthesis, characterization, and in vitro evaluation of novel ruthenium(II) η^6-arene imidazole complexes. *J. Med. Chem.* **2006**, *49*, 5552−5561.
(35) Ma, D.; Cai, Q. L-Proline promoted Ullmann-type coupling reactions of aryl iodides with indoles, pyrroles, imidazoles, or pyrazoles. *Synlett* **2004**, 128−130.
(36) Mosmann, T. Rapid colorimetric assay for cellular growth and survival: Application to proliferation and cytotoxicity assays. *J. Immunol. Methods* **1983**, *65*, 55−63.
(37) Weiss, J.; Dormann, S.-M. G.; Martin-Facklam, M.; Kerpen, C. J.; Ketabi-Kiyanvash, N.; Haefeli, W. E. Inhibition of P-glycoprotein by newer antidepressants. *J. Pharm. Exp. Ther.* **2003**, *305*, 197−204.
(38) Allardyce, C. S.; Dorcier, A.; Scolaro, C.; Dyson, P. J. Development of organometallic (organo-transition metal) pharmaceuticals. *Appl. Organomet. Chem.* **2005**, *19*, 1−10.
(39) (a) Pigeon, P.; Top, S.; Vessières, A.; Huché, M.; Hillard, E. A.; Salomon, E.; Jaouen, G. Selective estrogen receptor modulators in the ruthenocene series. Synthesis and biological behavior. *J. Med. Chem.* **2005**, *48*, 2814−2821. (b) Top, S.; Vessières, A.; Pigeon, P.; Rager, M.-N.; Huché, M.; Salomon, E.; Cabestaing, C.; Vaissermann, J.; Jaouen, G. Selective estrogen-receptor modulators (SERMs) in the cyclopentadienylrhenium tricarbonyl series: Synthesis and biological behaviour. *ChemBioChem* **2004**, *5*, 1104−1113. (c) Top, S.; Kaloun, E. B.; Vessières, A.; Leclercq, G.; Laïos, I.; Ourevitch, M.; Deuschel, C.; McGlinchey, M. J.; Jaouen, G. Tamoxifen derivatives for delivery of the antitumoral (DACH)Pt group: Selective synthesis by McMurry coupling, and biochemical behaviour. *ChemBioChem* **2003**, *4*, 754−761. (d) Top, S.; Vessières, A.; Leclercq, G.; Quivy, J.; Tang, J.; Vaissermann, J.; Huché, M.; Jaouen, G. Synthesis, biochemical properties, and molecular modelling studies of organometallic specific estrogen receptor modulators (SERMs), the ferrocifens and hydroxyferrocifens: Evidence for an antiproliferative effect of hydroxyferrocifens on both hormone-dependent and hormone-independent breast cancer cell lines. *Chem.−Eur. J.* **2003**, *9*, 5223−5236. (e) Top, S.; Kaloun, E. B.; Vessières, A.; Laïos, I.; Leclercq, G.; Jaouen, G. The first titanocenyl dichloride moiety vectorised by a selective estrogen receptor modulator (SERM). Synthesis and preliminary biochemical behaviour. *J. Organomet. Chem.* **2002**, *643*, 350−356.
(40) (a) Delhaes, L.; Biot, C.; Berry, L.; Delcourt, P.; Maciejewski, L. A.; Camus, D.; Brocard, J. S.; Dive, D. Synthesis of ferroquine enantiomers: First investigation of effects of metallocenic chirality upon antimalarial activity and cytotoxicity. *ChemBioChem* **2002**, *3*, 418−423. (b) Domarle, O.; Blampain, G.; Agnaniet, H.; Nzadiyabi, T.; Lebibi, J.; Brocard, J.; Maciejewski, L.; Biot, C.; Georges, A. J.; Millet, P. In vitro antimalarial activity of a new organometallic analog, ferrocene-chloroquine. *Antimicrob. Agents Chemother.* **1998**, *42*, 540−544. (c) Biot, C.; Glorian, G.; Maciejewski, L. A.; Brocard, J. S. Synthesis and antimalarial activity in vitro and in vivo of a new ferrocene-chloroquine analogue. *J. Med. Chem.* **1997**, *40*, 3715−3718.
(41) Barnes, K. R.; Kutikov, A.; Lippard, S. J. Synthesis, characterization, and cytotoxicity of a series of estrogen-tethered platinum(IV) complexes. *Chem. Biol.* **2004**, *11*, 557−564.
(42) Ang, W. H.; Khalaila, I.; Allardyce, C. S.; Juillerat-Jeanneret, L.; Dyson, P. J. Rational design of platinum(IV) compounds to overcome glutathione-S-transferase mediated drug resistance. *J. Am. Chem. Soc.* **2005**, *127*, 1382−1383.
(43) (a) Streu, C.; Meggers, E. Ruthenium-induced allylcarbamate cleavage in living cells. *Angew. Chem., Int. Ed.* **2006**, *45*, 5645−5648. (b) Atilla-Gokcumen, G. E.; Williams, D. S.; Bregman, H.; Pagano, N.; Meggers, E. Organometallic compounds with biological activity: A very selective and highly potent cellular inhibitor for glycogen synthase kinase 3. *ChemBioChem* **2006**, *7*, 1443−1450. (c) Bregman, H.; Carroll, P. J.; Meggers, E. Rapid access to unexplored chemical space by ligand scanning around a ruthenium center: Discovery of potent and selective protein kinase inhibitors. *J. Am. Chem. Soc.* **2006**, *128*, 877−884. (d) Bregman, H.; Williams, D. S.; Atilla, G. E.; Carroll, P. J.; Meggers; E. An organometallic inhibitor for glycogen synthase kinase 3. *J. Am. Chem. Soc.* **2004**, *126*, 13594−13595.
(44) Bennett, M. A.; Huang, T.-N.; Matheson, T. W.; Smith, A. K. (η^6-Hexamethylbenzene) ruthenium complexes. *Inorg. Synth.* **1982**, *21*, 74−78 (Fackler, J. P., Jr., Ed.).
(45) Gottlieb, H. E.; Kotlyar, V.; Nudelman, A. NMR chemical shifts of common laboratory solvents as trace impurities. *J. Org. Chem.* **1997**, *62*, 7512−7515.
(46) Dyson, P. J.; McIndoe, J. S. Analysis of organometallic compounds using ion trap mass spectrometry. *Inorg. Chim. Acta* **2003**, *354*, 68−74.
(47) Ang, W. H.; Pilet, S.; Scopelliti, R.; Bussy, F.; Juillerat-Jeanneret, L.; Dyson, P. J. Synthesis and characterization of platinum(IV) anticancer drugs with functionalized aromatic carboxylate ligands: Influence of the ligands on drug efficacies and uptake. *J. Med. Chem.* **2005**, *48*, 8060−8069.
(48) Hanessian, S.; Zhan, L. J.; Bovey, R.; Saavedra, O. M.; Juillerat-Jeanneret, L. Functionalized glycomers as growth inhibitors and inducers of apoptosis in human glioblastoma cells. *J. Med. Chem.* **2003**, *46*, 3600−3611.
(49) Duisenberg, A. J. M. Indexing in single-crystal diffractometry with an obstinate list of reflections. *J. Appl. Cryst.* **1992**, *25*, 92−96.
(50) Oxford Diffraction. *CrysAlis CCD* and *CrysAlis RED*, versions 1.170; Oxford Diffraction Ltd.: Abingdon, Oxfordshire, U. K., 2003.
(51) Hooft, R. W. W. *CollectCCD*; Nonius BV: Delft, Netherlands.
(52) Sheldrick, G. M. *SADABS*; program for empirical absorption correction of area detector data; University of Göttingen: Göttingen, Germany, 1996.
(53) Spek, A. L. Single-crystal structure validation with the program PLATON. *J. Appl. Cryst.* **2003**, *36*, 7−13.
(54) Bruker. *XPREP*, version 6.14; Bruker AXS, Inc.: Madison, Wisconsin, U.S.A., 2003.
(55) Sheldrick, G. M. *SHELXS97* and *SHELXL97*; University of Göttingen: Göttingen, Germany, 1997.
(56) Farrugia, L. J. ORTEP-3 for Windows, a version of ORTEP-III with a graphical user interface (GUI). *J. Appl. Cryst.* **1997**, *30*, 565.

JM070039F